Pervious concrete with secondarily recycled low-quality brick-concrete demolition residue: engineering performances, multi-scale/phase structure and sustainability

Nidu Jike[a], Chengji Xu[a], Rijiao Yang[a], Yuxuan Qi[a], Yuqing Dai[a],

Yu Peng[a], Jiyang Wang[a], Mingzhong Zhang[b], Qiang Zeng[a] *

(a) College of Civil Engineering and Architecture, Zhejiang University, Hangzhou 310058, P.R. China.

(b) Department of Civil, Environmental and Geomatic Engineering, University College London, London, WC1E 6BT, UK

*Corresponding author, cengq14@zju.edu.cn

Abstract:

Brick-concrete demolition residue after the primary recycling is generally discarded due to its low quality. Secondary recycling of the brick-concrete demolition residue is urgently required to be solved at present in China due to the large scale constructions and demolitions, and remains a challenging task. In this work, a brick-concrete demolition residue from an urban-fringe of Hangzhou, China, was secondarily recycled as the fine aggregate to fabricate sustainable pervious concrete after systematic characterization of its physical and chemical properties. In order to improve the engineering properties of the pervious concrete, natural aggregate and sand were used. Multi-scale structure in terms of pore size distribution, skeleton

morphology, and matrix-aggregate interfacial transition zone were systematically characterized using X-ray computed tomography and backscattered electron imaging tests. Results show that the increase of the natural aggregate replacement ratio and sand ratio always increases the compressive strength and density, but decrease the water permeability. Incorporation of secondary brick-concrete demolition residue in concrete increases the total porosity and connected porosity of the pervious concrete, and helps form the Calcium-enriched matrix-aggregate interfacial layer zone. Use of the secondarily recycled brick-concrete demolition residue in pervious concrete manufacture at the optimal mix brings the CO_2 emissions reduction by 107 kg/m^3 and costs reduction by 30.3 USD/m^3. The findings of this work provide a sustainable route to secondarily recycle low-quality brick-concrete demolition residue for constructions.

Keywords:

Demolition residue; Secondary recycling; Pervious concrete; XCT; Sustainability; CO_2 emission.

1. Introduction

1.1 Literature review

The generation of construction and demolition waste (CDW) has been accelerated in China triggered by the population growth, booming economy, and rapid urbanization. Over 2.3 billion tons of CDW was annually generated in China according to an estimation (Yazdani et al., 2021), and majority of the CDW was piled up at rural area or simply sent to landfill due to the low recycling rate (around 5%), which brings pollutions to the soil, air and water in urban areas (Ahmed Shaikh et al.,

2019; Li et al., 2020). Given the important part the CDW plays, improving the utilization efficiency of CDW in China is one of the key ways to achieve high sustainability for China's urban developments. Difficulties in CDW recycling efficiency rise due to the huge variances in CDW source and quality (Ma et al., 2020). At present, the uses of high-quality CDW with high mechanical properties and volume stability, such as concrete block, brick and ceramic, have been widely employed for concrete manufacture (Robalo et al., 2021). For low-quality CDW, such as, the brick-concrete demolition residue (BCDR) after a primary recycling, it is eventually discarded in landfill. The efficient secondary recycling of BCDR is a new issue and a challenging task in concrete community and industry.

From available reports, the recycling and reuse of inert CDW phase as construction and building materials (CBMs) is favorable for its huge potential to reduce pollutions, landfills, and consumptions of natural aggregate, resulting in the benefits of less energy consumption and CO_2 emissions (Ahmed Shaikh et al., 2019; Liu et al., 2020; Ma et al., 2020; Yazdani et al., 2021). An estimation showed that the use of CDW as coarse aggregate is beneficial to decrease the CO_2 emission of concrete by over 24% (Yap et al., 2018). Moreover, the recycled ~~CD waste~~ CDW powder may be used as supplementary cementations materials (SCM) to partially replace the cement for concrete manufacture, which will further promote the sustainability of concrete (Duan et al., 2020; Sun et al., 2021). In a word, the use of ~~CD waste~~ CDW in concrete can enhance the sustainability of construction industry in

both the economic and environmentally friendly measure (Olofinnade and Ogara, 2021; Robalo et al., 2021).

In the measure of engineering performances, however, the use of ~~CD waste~~ CDW, especially the secondary low-quality BCDR after primary recycling, generally lowers concrete's grade, bringing difficulties in structural applications (Zhang et al., 2021). Thus, focuses are put on the non-structural applications of CDW with relatively low criteria of mechanical and durability properties, e.g., pervious concrete (Neithalath et al., 2010). Compared with traditional solid concrete with limited porosity, pervious concrete with relatively high connected porosity (15-35%) (Deo and Neithalath, 2010; Putman and Neptune, 2011; Yang and Jiang, 2003) possesses many environmental benefits, such as controlling rainwater runoff, restoring groundwater supply, improving water quality, and reducing soil pollution (Otter et al., 2016; Park et al., 2014). As an environmentally friendly paving material, pervious concrete has been increasingly used in the development of low-capacity pavements such as sidewalks, parking lots, and alleys (Chandrappa and Biligiri, 2016). According to the U.S. Environmental Protection Agency (EPA), pervious concrete may be one of the best materials to mitigate rainwater runoff in urban areas (Neithalath et al., 2010). The porous structure of pervious concrete for pavement constructions offers benefits of adjustment of the temperature and humidity of the earth's surface and mitigation of the heat island phenomenon in cities (Yang and Jiang, 2003). Moreover, the high absorbing capacity of noise by pervious concrete pavement can greatly improve the living environment (Kim and Lee, 2010).

Given the great sustainability of the substitution of natural aggregate with ~~CD waste~~ CDW and the multiply environmental benefits of pervious concrete, the secondary recycling of BCDR for pervious concrete fabrication would bring synergistic sustainability improvement. Indeed, great efforts have been made to recycle wastes from the industries of mining, power, construction, and agriculture, as either the aggregates and/or the fillers to fabricate pervious concrete (Table 1). It is clear that huge data variances show up in strength and water permeability, ~~which are the~~ two most important factors affecting the engineering performances of pervious concrete (Chindaprasirt et al., 2009; Yu et al., 2019a, b; Zhong and Wille, 2016). Many techniques/methods were therefore proposed to improve the strength and permeability of pervious concrete with recycled aggregate, such as, use of silica fume (Chaitanya and Ramakrishna, 2021), fly ash (Vieira et al., 2020), slag (El-Hassan et al., 2019), and pumice powder and nano-clay (Mehrabi et al., 2021). However, owing to the specific features of BCDR (e.g., lower strength, rougher surfaces, higher water absorption and heavier graded particle size), difficulty arises in tuning the mechanical properties and water permeability of pervious concrete with secondarily recycled BCDR aggregate. It is therefore important to address the multi-scale structure of pervious concrete with low-quality BCDR and its relationships with the mechanical properties and permeability.

Table 1 Pervious concrete fabrication with different recycled aggregates

Reference	Aggregate type	Strength (MPa)	Permeability (cm/s)

Reference	Aggregate type	Strength (MPa)	Permeability (cm/s)
Shen et al., 2021	Incineration bottom ash	20	0.06
Zhang et al., 2020	Steel slag	32	1.3
Bittencourt et al., 2021	Recycled asphalt	3.7	1.0
Debnath and Sarkar, 2020	Over burnt brick	3-10	1.2-2.1
Sherwani et al., 2021	Artificial fly-ash	11.1	0.93
Shen et al., 2020	Waste glass	33	0.07
Lori et al., 2019	Copper slag	23.45	0.336
Liu et al., 2020	Sterculia foetida petiole waste	9-13	1.44-3.0
Ibrahim et al., 2020	Recycled concrete	11	2.53
El-Hassan et al., 2019	Recycled concrete	3-37	0.2-2.1
Chaitanya and Ramakrishna, 2021	Recycled concrete	3.16-3.87	0.88-1.63
Mehrabi et al., 2021	Recycled concrete	2.8-28	2.1-3.5
Vieira et al., 2020	CDW	3-13	0.35-0.75

1.2 Background of this study

Triggered by the Asian Games 2022, a large number of construction projects have been launched and are ongoing in the urban fringes of Hangzhou, China. Fig. 1 demonstrates the rapid changes in urban landscape of a local urban-fringe in Gongshu district of Hangzhou, China, between June 2019 and April 2021. The ongoing high-strength constructions result in massive CDW, bringing high stresses to the environments.

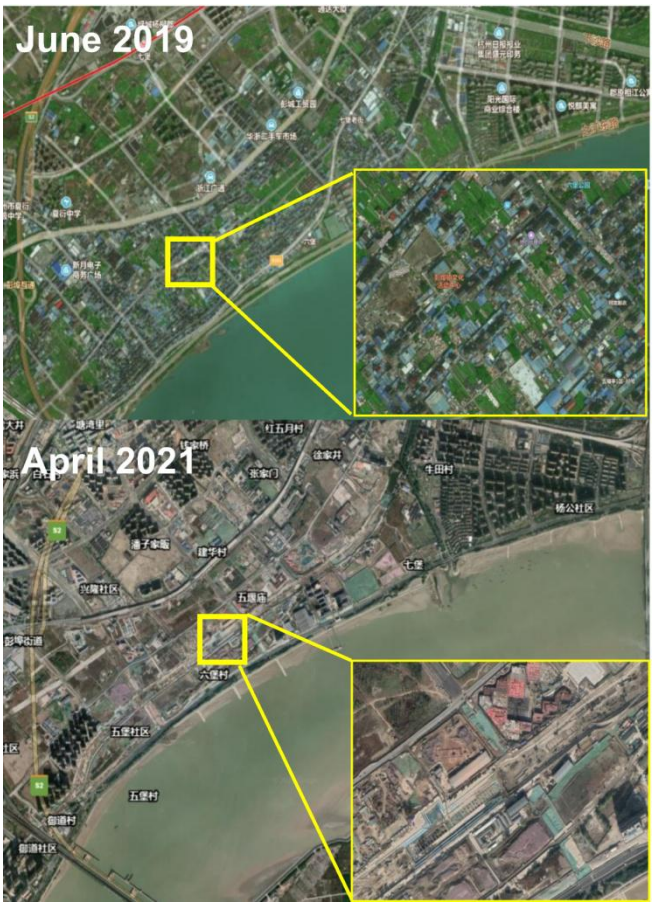

Figure 1. Changes in urban landscape of a local urban-fringe in Gongshu district of Hangzhou, China, between June 2019 and April 2021.

Because most of the demolished buildings built by local people in 10-30 years ago were in masonry-concrete structure, the demolition waste mostly consists of bricks and concrete. An in-situ survey suggested that a portion of the CDW has been recycled in certain ways. A recycling factory was established once these projects began between 2016-2018. Most of the undamaged bricks with complete appearance were directly recycled in the followed constructions, while the damaged bricks, concrete blocks and other inerts were crushed, sieved, and partially recycled. The inerts with particle size between 10 and 45 mm were recycled as coarse aggregate after washing. The total efficiency of the primary recycling varies from 65%-80

127 depending on the quality of demolitions. The rest BCDR cannot be directly recycled
128 due to its low quality, and thus the ongoing pileup of large scale of those low-quality
129 BCDR is an urgent problem to be solved before the opening of the Asian Games 2022.
130 This thus provides strong incentives to explore new routes to secondarily recycle the
131 BCDR for CBM applications.

132 **1.3 Significance and content of this study**

133 In the present work, ~~we aim at~~ it is aimed at mitigating the rapid growth of low-
134 quality BCDR after a primarily coarse recycling. BCDR was further recycled as the
135 fine aggregate to develop sustainable pervious concrete. Eighteen mixes were
136 designed to comprehensively investigate the effect of natural aggregate substitution
137 ratio and sand ratio on the engineering performances of pervious concrete. Multi-scale
138 structures of pores, skeletons and matrix-aggregate interfacial transition zones (ITZs)
139 were characterized by X-ray computed tomography (XCT) and scanning electron
140 microscopy (SEM) with backscattered electron (BSE) model. Pore size distribution
141 (PoSD) and connected porosity were specifically studied. The thickness of
142 cementitious mortar on the BCDR aggregates were quantitatively evaluated. The
143 nexus among porosity, strength and water permeability was discussed. The
144 sustainability of pervious concrete with the secondarily recycled BCDR fine
145 aggregate in terms of CO_2 emissions and the economic benefits were assessed. The
146 findings of this work would facilitate the rational mix design of pervious concrete
147 incorporating the secondarily recycled low-quality CDW to balance the mechanical
148 properties and water permeability with improved sustainability, and provide novel

149 solutions to mitigate the environmental stresses by the continual piling up of large
150 amount of CDW residue..

151 **2. Materials and Methods**

152 ***2.1 Characterization of BCDR***

153 Most of the resident buildings in south-eastern areas of China are built in
154 masonry structure, so brick and concrete may contribute mostly to the demolition
155 waste. Fig. 2a shows a picture of typical demolitions from masonry resident buildings.
156 After recycling the bricks with complete appearance and the coarse demolition
157 particles over 10 mm, the residue of the brick-concrete demolition was collected for
158 further processing (Fig. 2b). The low-quality CDW residue, collected from a local
159 recycling factory, was immersed in water to remove the light materials such as woods
160 and foam plastics. The rest sediments were dried in a solar drying process for at least
161 3 days. After that, the CDW residue was sieved in a sieving system according to GB/T
162 25176 (2010). Particle size distribution (PaSD) of the BCDR was analyzed by a
163 sieving system. Around three-quarter of the BCDR is larger than 1.18 mm (74%wt)
164 (Fig. 2c), which may be used as the fine aggregate for the secondary recycling in
165 pervious concrete fabrication (ASTM C33/C33M-16). The rest one-quarter of the
166 BCDR with particle size below 1.18 mm (26%wt) was discarded, because it cannot be
167 directly used for concrete manufacture. Primary tests indicated that the complete use
168 of BCDR can cause higher water demands and significant pore clogs due to the filling
169 effect of the particles thinner than 1.18 mm.

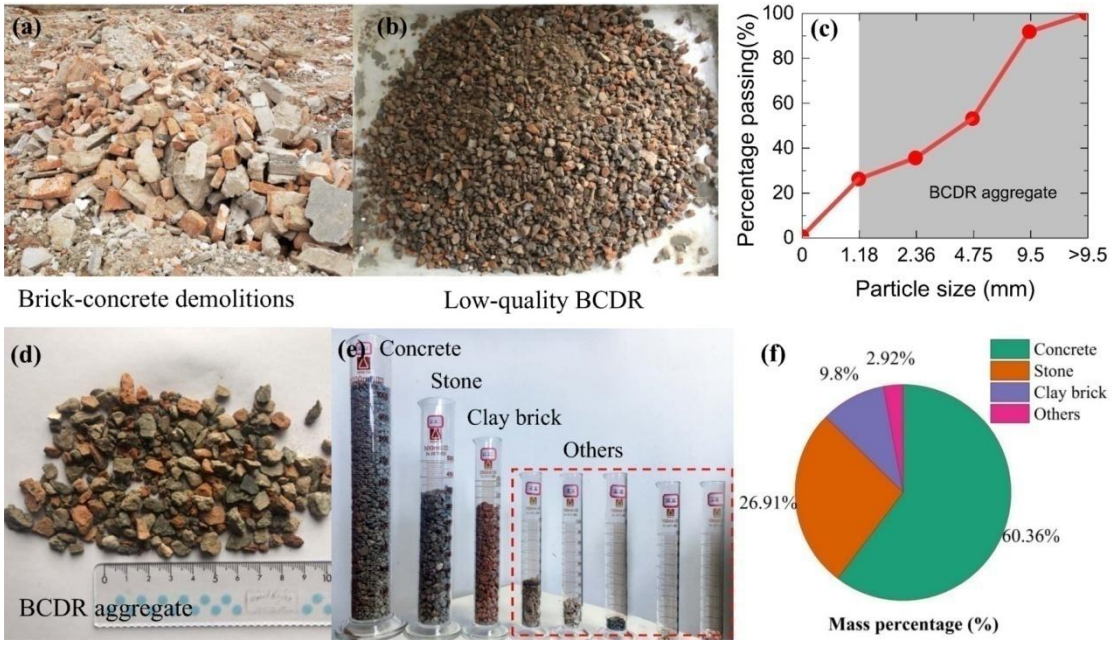

170

171 **Figure 2.** (a) Typical raw brick-concrete demolitions from masonry resident buildings, (b) BCDR
172 after the primary recycling, (c) Particle size distribution of the BCDR, (d) image of selected
173 BCDR aggregate after particle size threshold at 1.18 mm (particles over 1.18 mm), (e) volume and
174 (f) mass distribution of different phases (recycled concrete, stone, clay brick and other inerts).

175 A typical image of the BCDR aggregate is shown in (Fig. 2d). Clearly, the
176 recycled BCDR aggregate is a mixture of different solids, including, recycled concrete,
177 stone, clay brick, and other inerts. Manual classification on 2 kg of the BCDR
178 aggregate was conducted for component analysis. The recycled concrete, stone and
179 clay brick occupy over 94% by volume and 96% by mass (Fig. 2e and f). Few
180 decoration material residue like gypsum, as well as ceramics, wood and metals, can be
181 found in the BCDR aggregate.

182 A type of granite natural aggregate with the same particle size distribution was
183 used for comparison. The physical properties and engineering indexes of both natural
184 and BCDR aggregates were tested according to GB/T 25176 (2010) and GB/T 25177

(2010) (Table 2). The water absorption and crushing index of the BCDR aggregate are 15.30% and 15.94%, respectively, significantly higher than the values of 1.52% and 9.80% for natural aggregate (Table 2). According to the criteria of recycled aggregates in the Chinese standards (GB/T 25177, 2010) and (GB/T 50743, 2012), the water absorption of recycled aggregate should be lower than 8% and 10%, respectively. Therefore, the BCDR solids are not qualified as the recycled aggregate used in ordinary concrete, but may be a preferable candidate for pervious concrete manufacture.

Table 2. Physical properties of the BCDR and natural aggregates.

Physical properties	BCDR aggregate	Natural aggregate
Particle size (mm)	1.18-9.5	2.36-9.5
Apparent density (kg/m^3)	2536.3	2883.4
Bulk density (kg/m^3)	1345.1	1560.2
Moisture content (%)	3.2	1.0
Water absorption (%)	15.3	1.52
Crush index (%)	15.94	9.8

2.2 Experimental design

A type of Portland cement (PII 52.5) was used as the binding material for previous concrete fabrication, and its density and specific surface area are 3.13 g/cm^{3}and 346 m^2/kg, respectively.

Primary tests indicated that the strength of pervious concrete samples with 100% BCDR aggregate was too low to meet the engineering requirements, so two schemes

were designed to improve the mechanical properties: 1) using natural aggregate to partially replace BCDR aggregate, and 2) adding sand to tune aggregate gradation (Bonicelli et al., 2015). A river sand with the fineness of 2.6 was used.

A total of 18 mix proportions were designed for pervious concrete fabrication based on ACI 522R (2010) (Table 3). Six levels of natural aggregate substitution ratio, i.e., 0%, 20%, 40%, 60%, 80% and 100%, and three levels of sand content (measured by sand-to-cement ratio, S/C), i.e., 0,0.5 and 1, were set. Higher S/C ratio can enhance strength but greatly induce pore clogging (ACI 522R, 2010). In all mixes, the amount of superplasticer (SP, Sika-II hydroxypropyl methylcellulose, Sika, Switzerland) was kept constant (1% of the cement). Due to the huge differences in water absorption between the BCDR aggregate and nature aggregate, a fixed water-to-binder (W/B) ratio cannot maintain the same state of different mixes. Therefore, the principle of controlling the same liquidity was applied to adjust the water consumption with trials and errors. The w/b ratio of the initial trial was 0.2, and increased slowly by a step of 0.005 till the best consistency. The final mix proportions of the pervious concrete are shown in Table 3.

Table 3. Mix proportions of the pervious concrete (kg/m^3).

Sample ID	Cement (kg)	BCDR aggregate (kg)	Natural aggregate (kg)	Sand (kg)	Water (kg)	SP (kg)	W/B	S/C
PC0	205.69	1028.47	0.00	0.00	123.42	2.05	0.6	0
PC20	209.22	836.86	209.22	0.00	104.61	2.09	0.5	0
PC40	201.88	605.64	403.76	0.00	80.75	2.02	0.4	0

PC60	188.02	376.03	564.05	0.00	56.40	1.88	0.3	0
PC80	181.09	181.09	724.37	0.00	42.56	1.81	0.235	0
PC100	173.50	0.00	867.52	0.00	40.77	1.74	0.235	0
PC0S0.5	249.79	1124.05	0.00	124.89	99.92	2.50	0.4	0.5
PC20S0.5	234.51	844.24	211.06	117.26	77.39	2.35	0.33	0.5
PC40S0.5	225.96	610.09	406.72	112.98	67.79	2.26	0.3	0.5
PC60S0.5	219.80	395.65	593.47	109.90	54.95	2.20	0.25	0.5
PC80S0.5	209.45	188.51	754.03	104.73	46.08	2.09	0.22	0.5
PC100S0.5	212.49	0.00	956.20	106.24	42.50	2.12	0.20	0.5
PC0S1	283.56	1134.22	0.00	283.56	141.78	2.84	0.5	1
PC20S1	276.43	884.59	221.15	276.43	124.40	2.76	0.45	1
PC40S1	252.54	606.10	404.06	252.54	94.70	2.53	0.375	1
PC60S1	250.32	400.51	600.77	250.32	87.61	2.50	0.35	1
PC80S1	239.90	191.92	767.67	239.90	71.97	2.40	0.3	1
PC100S1	229.60	0.00	918.41	229.60	68.88	2.30	0.3	1

2.3 Preparation of pervious concrete

Pervious concrete specimens were prepared according to JCT 2558 (2020). During the mixing processes, the aggregates (BCDR aggregate and/or natural aggregate) and cement were dry-mixed in a mixer for 1 min. Water was slowly added into the mixer with progressive manual trails (Fig. 3a). An appropriate material status was achieved (Fig. 3b) when the fresh concrete can gather together to form a sticky agglomeration after being lightly compacted in the palm of the hand (Xie et al., 2018).

The readily prepared fresh pervious concrete was cast into cubic and cylindrical moulds. To avoid the possible pore clogging caused by the sinking of flowable cement paste, no vibrations were conducted to all specimens. Instead, manual compression

was used during the casting of the pervious concrete specimens (Zhou, 2018). After surface finishing, all the specimens' open surfaces were sealed with a layer of plastic film to prevent moisture loss (Fig. 3c). The specimens, together with the molds, were stored in a chamber at 23 ℃ for primary curing.

Figure 3 The fabrication processes of pervious concrete: (a) wet status of pervious concrete, (b) manual examination in hand, (c) casting of fresh pervious concrete in cubic and cylinder moulds, (d) pervious concrete specimens stored in a chamber, and illustration of selected (e) cubic and (f) cylindrical specimens.

After the primary curing for 24 h, the specimens were demoulded and cured in standard curing conditions (temperature of 20 ± 2 ℃and relative humidity > 95 %) (Fig. 3d). At set ages, the concrete cubes (with the side length of 100 mm, Fig. 3e) and cylinders (with the diameter of 100 mm and length of 200 mm, Fig. 3f) were readily prepared for the compressive and water permeability tests, respectively. For each mix,

9 samples were tested with 6 for strength (7 d and 28 d), and 3 for density and permeability (28 d); for the mixes with S/C=0.5, additional 6 samples were selected for XCT and SEM tests (28 d). In total, 168 samples were consumed for all tests.

2.4 Methods

2.4.1 Compressive strength

Strength tests of the pervious concrete were conducted according to the Chinese standard of JCT 2558-2020. At the curing ages of 7 d and 28 d, concrete cubes were removed from the chamber to experience compression tests. An Instron 8802 full functional electro-hydraulic servo test machine was applied to exert forces on the cubic specimens at 0.35 kN/s. The maximum forces recorded were adopted to calculate compressive strength. Three independent tests were repeated for each mix at each age, and the data were averaged to obtain the reliable compressive strength.

2.4.2 Water permeability

For water permeability test, a falling water head (FWH) permeability method was applied according to GB/T 25993 (2010). The FWH method is a commonly used for water permeability tests due to its high reliability and convenience (Lori et al., 2019; Neithalath et al., 2010). For each FWH test, when water head fell from an initial head (h_1) to a set final head (h_2), the duration time was recorded (t), then the permeability coefficient can be estimated as $k = \ln(h_2/h_1)\, l/t$, where l is the length of the specimen (150 mm), t is the time for water head fall. Here the initial and final water heads were 290 mm and 70 mm, respectively, so the water permeability

coefficient can be simply estimated as: $k = 21.32/t$ (cm/s). For each mixture, three FWH tests were repeated to measure the water permeability coefficient.

2.4.3 X-Ray computed tomography

XCT, as a non-destructive testing technique, has been widely used to characterize the pore structure (Zeng et al., 2020), explore the relationship between pore size and mechanical properties (Yu et al., 2019; Zhou et al., 2019), and analyze the pore connectivity and the paths for simulating the seepage of pervious concrete (Zhang et al., 2018). Here, an industrial XCT device of XTH255/320 LC (Nikon, Japan) was applied for XCT scans. A voltage of 180 kV and a current of 160 μA were used to emit X-ray beams. During XCT test, a pervious concrete cylinder was fixed on the sample frame, and rotated evenly by 360 degrees in 1500 s during the emissions of X-ray beams (Fig. 4a). Massive X-ray transmission projections at different angles were recorded by a high-resolution detector (2000 h × 2000 v) and stored in computer. The exposing time for each projection was 0.75 s, and a total of 2000 projections were generated for the complete scans of each sample (Fig. 4b).

A CTPro software was used to read the X-ray images and reconstruct the digital object (Fig. 4c). The pixel size of the X-ray images was 55 μm. The XCT data were then loaded into a VGSTUDIO MAX software for further data processing including selection of region-of-interest (ROI), threshold for phase segmentation, and microstructure reconstruction (Fig. 4d and e). The phase segmentation relies on the mechanism that lightweight phases with low X-ray attenuations (such as, pores, woods and plastics) are shown in high darkness and low gray values, while heavy

phases with high X-ray attenuations (such as, aggregates, cement pastes and metals) are displayed in low darkness with high gray values (Qi et al., 2021; Zeng et al., 2019).

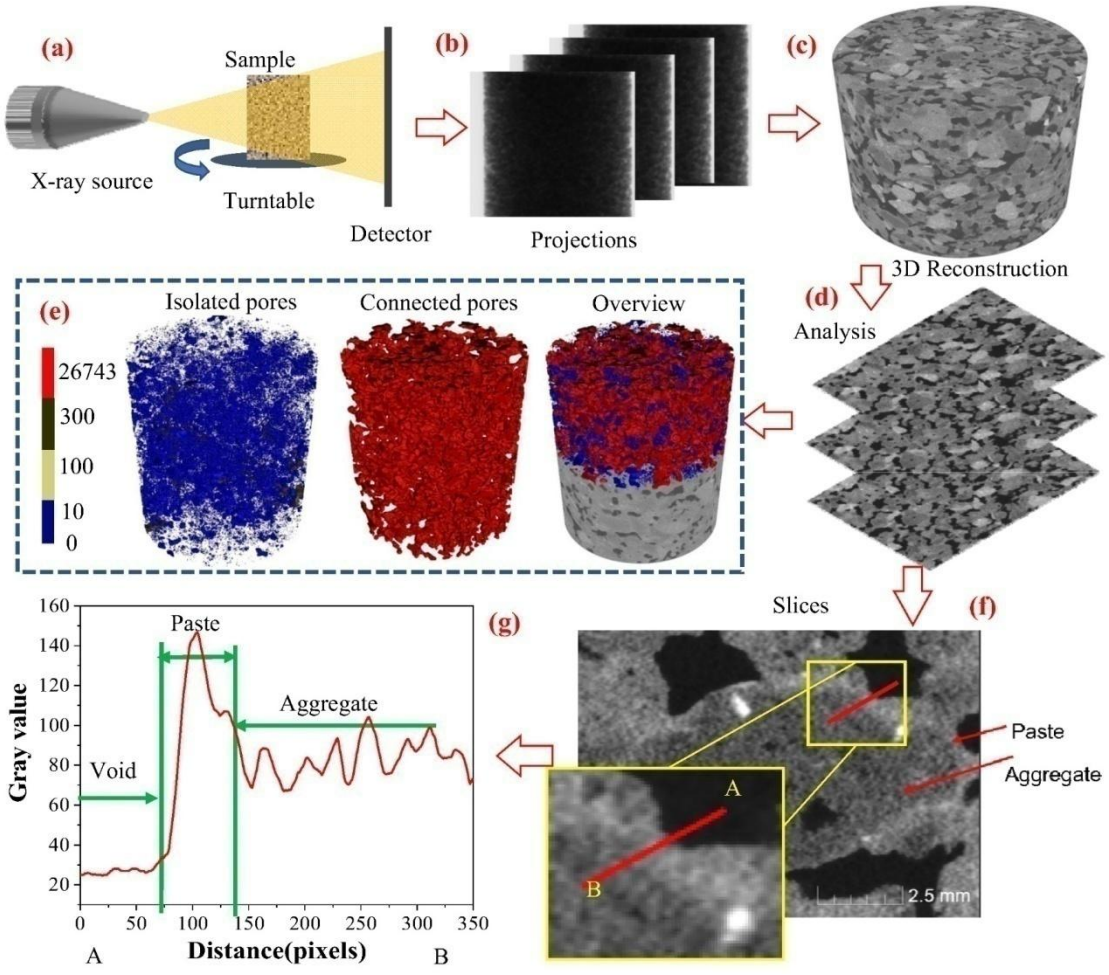

Figure 4. Schematic diagram of XCT test and pore structure analysis: (a) XCT scans of an object, (b) acquisition of X-ray projections; (c) 3D reconstruction of the object; (d) phase segmentation and analysis of local areas; (e) pore structure analysis in terms of overview, connected pores and isolated pores; (f) selection of local area for elaborate phase analysis; and (g) gray value distribution from pore to aggregate with phase reorganization.

The thickness of cement mortar on aggregates was quantified based on the gray value differences shown in XCT images. ROIs of local aggregates were selected (Fig

296 4f), and the analysis based on gray value gradients was performed via an ImageJ
297 software (Fig. 4g). For each sample, over 30 ROIs were selected and analyzed.
298 *2.4.4 SEM analysis*
299 A field emission environmental SEM (type of Quanta FEG650) equipped with an
300 energy-dispersed X-ray spectroscopy (EDS) system was employed for microstructure
301 analysis. Back-scattered electron (BSE) mode was applied in necessary for the
302 acquisition of high-quality BSE images for phase analysis. Small concrete segments
303 (around 10 mm) including both the BCDR aggregate and coating mortar were
304 collected from the central part of selected pervious concrete. After a sample
305 encasement process by epoxy resin, samples were polished by diamond papers in the
306 grade grits from 400# to 4000# in a Buehler semi-automatic polishing machine. All
307 samples were dried in an oven at 40℃ for 24 h to remove the capillary water. An
308 accelerating voltage of 20 keV was set during the SEM tests. Images at different
309 magnifications were acquired for the microstructure analysis of pores, cement
310 matrices and matrix-aggregate ITZs.
311 **3. Results and discussion**
312 ***3.1 Compressive strength***
313 Fig. 5 shows the compressive strength of all pervious concrete mixes. The
314 obtained strengths are all higher than the low limit of strength of pervious concrete
315 made with natural aggregate (3.5 MPa) reported in ACI 522R (2010). Apparently,
316 prolonging the curing age from 7 d to 28 d can systematically promote the
317 compressive strength (Fig. 5a-c) due to the continual hydration of cement that fill the

pores and bond together the aggregates (Yap et al., 2018). Decrease of the natural aggregate ratio (or rise of the BCDR ratio) always decreases the compressive (Fig. 5a-c), because the natural aggregate has higher strength and lower porosity than the BCDR aggregate. Similar findings are reported elsewhere (Olofinnade and Ogara, 2021; Yap et al., 2018; Zhang et al., 2017).

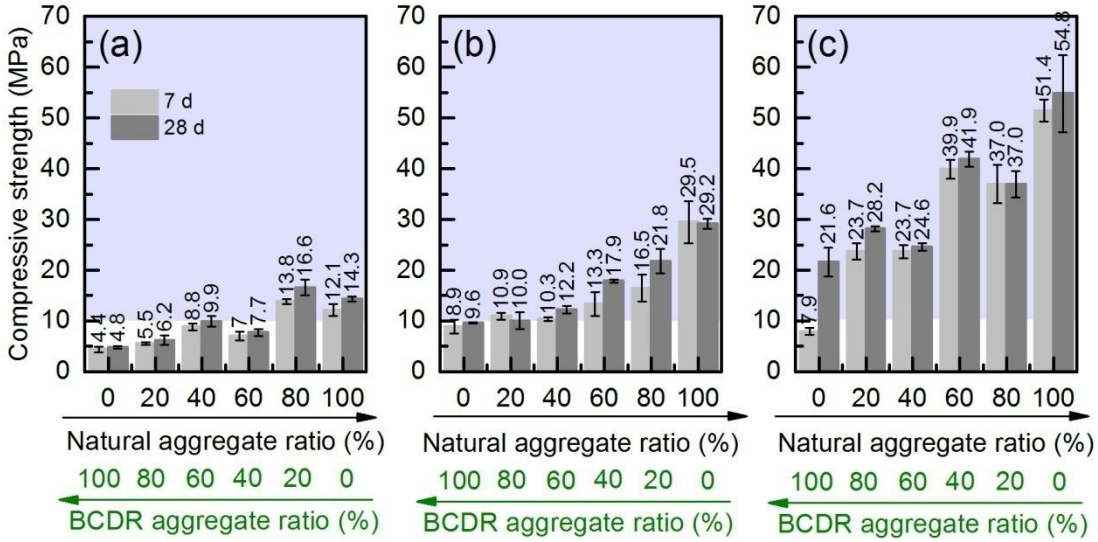

Figure 5 Compressive strength of pervious concrete at (a) S/C=0, (b) S/C=0.5, and (c) S/C=1.

In Fig. 5a, the specimens with S/C=0 show relatively low compressive strength (below 20 MPa). If a compressive strength of 10 MPa is set as the threshold for the applications of pavement (Yap et al., 2018), only the concrete mixes with 20% and 0% BCDR aggregate are qualified for the concrete mixes at S/C=0 (Fig. 5a). In this case, little amount of the low-quality BCDR can be recycled. To improve the compressive strength of pervious concrete, more cement may be required to fill the rough surfaces of recycled aggregates and hence to enhance the bonding effects (Tu et al., 2006, Etxeberria et al., 2007). However, raising cement content would increase the cost of the final product and CO_2 emissions (Braga et al., 2017; Visintin et al., 2020).

Alternatively, adding small amounts of sand into pervious concrete may be more effective and sustainable (Lian and Zhuge, 2010; Bonicelli et al., 2015). Test results evidence the substantial compressive strength increases of the pervious concrete with sand (Fig. 5b and c). For example, for the specimens with 100% BCDR aggregate, the compressive strengths of PC0S0.5 and PC0S1 are raised to 9.6 MPa and 21.6 MPa at 28 d, substantially higher than that of 4.8 MPa for PC0. Furthermore, almost all concrete mixes at S/C=0.5 and S/C=1 at 28 d exceed the threshold strength of 10 MPa (Fig. 5b and c), owing to the dense compactness of the skeletons with fine aggregates (Yang and Jiang, 2003; Zaetang et al., 2016). However, due to the detrimental effect of using sand in pervious concrete on water permeability, a high sand content may be not recommended. Strength-permeability balance should be achieved for pervious concrete design (see section 3.2 for more discussion).

3.2 Density and water permeability

Uses of natural aggregate and/or sand in pervious concrete can substantially increase the density (Fig. 6). For the pervious concrete mixes without sand (S/C=0), as the nature aggregate ratio decreases from 100% to 0%, the density decreases from 1949.3 kg/m^3 to 1357.6 kg/m^3 (by 30%). When S/C is increased to 0.5 and 1, the densities are systematically increased by 8% ~ 18% and 19% ~ 36%, respectively (Fig. 6). The density increases are ascribed to the intrinsic higher density of the sand and natural aggregate as well as their enhancements to particle compactness of pervious concrete. According the density threshold of 1920 kg/m^3 (ACI 213, 2003), most of the pervious concrete mixes without sand can be classified as lightweight concrete (Fig.

6). For the pervious concrete mixes with S/C=0.5, the maximum natural aggregate content should be not higher than 40% to conform the density requirements of lightweight concrete.

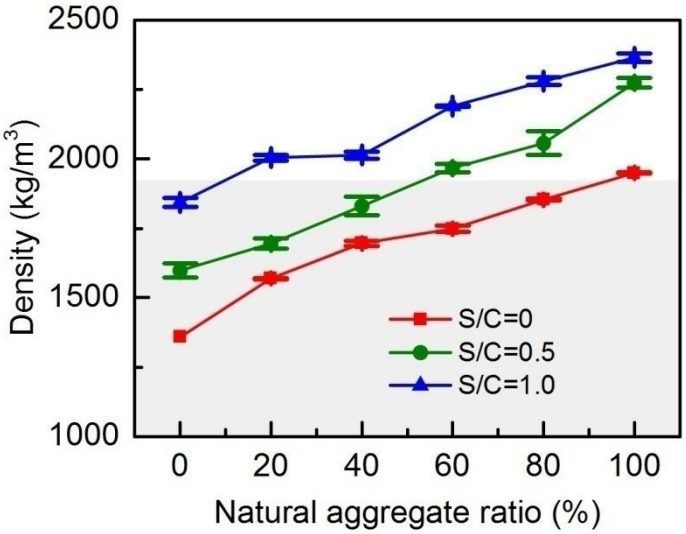

Figure 6 Density of all pervious concrete mixes

Fig. 7 shows the water permeability data of all pervious concrete mixes. For the mixes with S/C=0, 0.5 and 1, the water permeability coefficients are 0.06~0.12 cm/s, 0.02~0.05 cm/s and 0.001~0.005 cm/s, respectively. The great decrease of water permeability with increasing S/C ratio is certainly caused by the filling effect of sand particles that would thicken the cementitious coatings on aggregates and eliminate the pores for water permeation. According to the Chinese standard GB/T25993 (2010), pervious concrete with the water permeability > 0.01 cm/s and >0.02 cm/s can be sorted as B and A level, respectively. Accordingly, all concrete mixes with the S/C ratio of 1 cannot be classified as pervious concrete, because the water permeability values are lower than 0.01 cm/s. Meanwhile, the concrete series with the S/C ratios of

371 0 and 0.5, which show the water permeability over 0.02 cm/s except for PC100S0.5
372 (Fig. 7), may be applicable for permeable pavement casting.

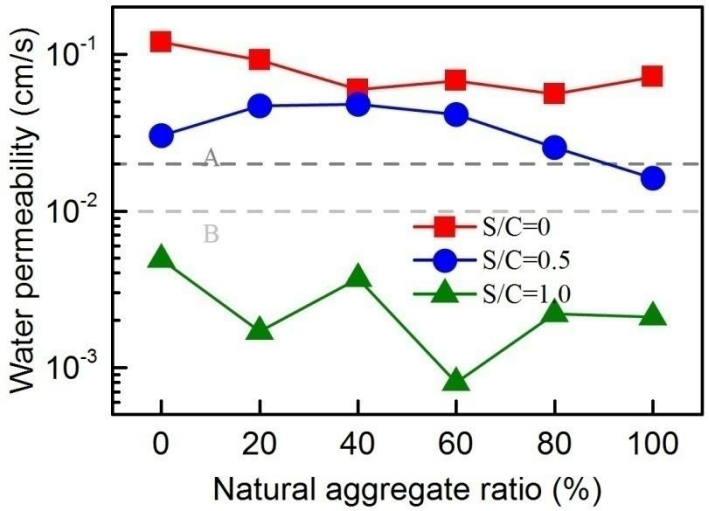

373

374 **Figure 7**. Water permeability of all pervious concrete mixes with the dashed lines A and B
375 indicating the water permeability levels of 0.02 cm/s and 0.01 cm/s, respectively

376 Considering both the compressive strength (Fig. 6) and water permeability (Fig.
377 7), one may conclude that the S/C ratio of 0.5 would bring the balanced engineering
378 properties of pervious concrete. Furthermore, the specimens with the BCDR
379 aggregates ratios between 40% and 80% (i.e., PC40S0.5, PC60S0.5 and PC80S0.5)
380 may show the optimal water permeability (0.041~0.048 cm/s) (Fig. 7). Therefore, in
381 what follows, focuses are shifted onto the pervious concrete series at S/C=0.5 with
382 multi-scale analyses.

383 ***3.3 Pore characteristics***

384 Total porosity of the pervious concrete mixes measured by weight method is
385 displayed in Fig. 8a. Like the water permeability trends shown in Fig. 7, a higher S/C
386 ratio induces a systematically lower total porosity, i.e., 22.5~37.3%, 8.0~26.5% and

5.2~10.9% for the pervious concrete mixes at S/C=0, 0.5 and 1, respectively. The trend consistency between water permeability and porosity is reported elsewhere (Neithalath et al., 2010; Sata et al., 2013).

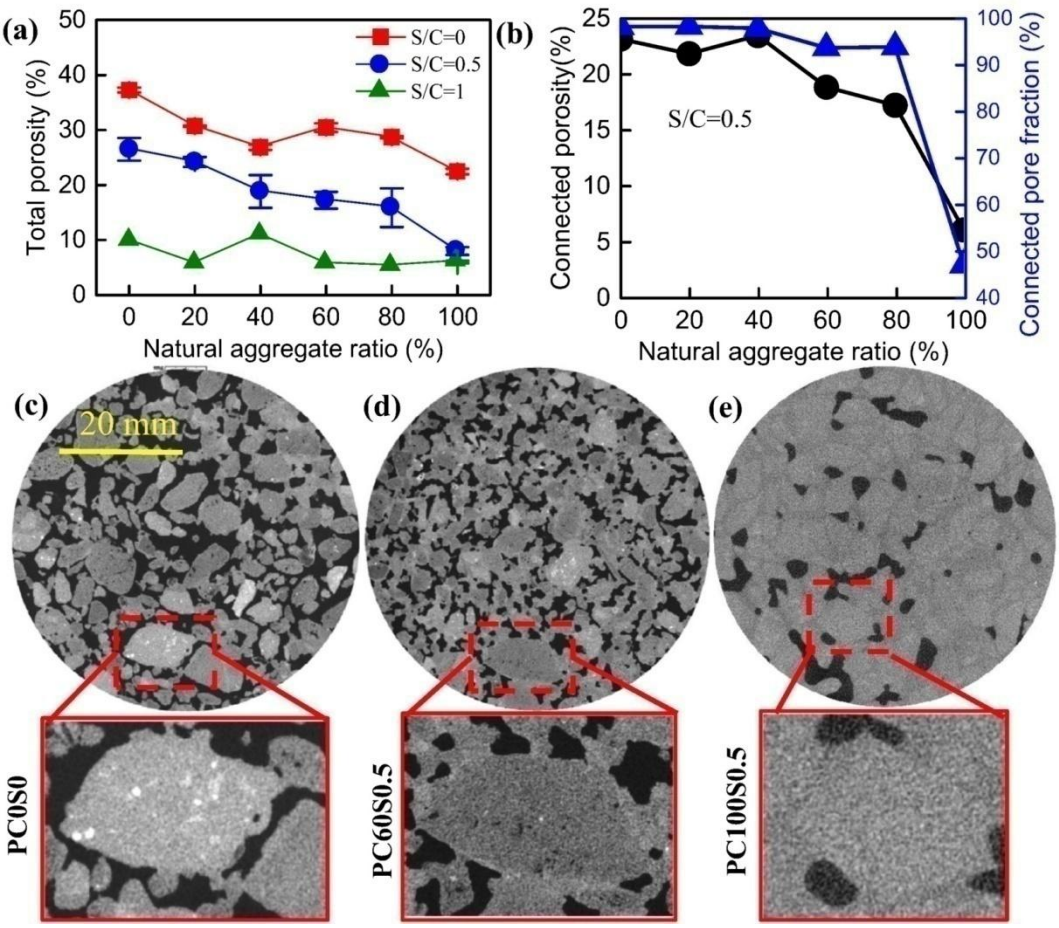

Figure 8 (a) Porosity measured by volumetric method; (b) connected porosity and its fraction to total porosity; (c-e) selected X-CT sections of PC0S0, PC60S0.5 and PC100S0.5.

To explore the water permeation mechanisms, the connected porosity of the pervious concrete mixes at S/C=0.5 analyzed by XCT is plotted in Fig. 8b. It shows slight and gent decreases in the connected porosity from 23% to 17% as the BCDR aggregate ratio decreases from 100% to 20%. A heavy decrease of the connected porosity to 4% emerges for the pervious concrete without BCDR aggregate (Fig. 8b).

The connected pore fraction, defined as the ratio of connected porosity to total porosity, shows the similar trend (Fig. 8b). The relatively low connected porosity and pore fraction of PC100S0.5 concrete also explain its low water permeability (Fig. 7).

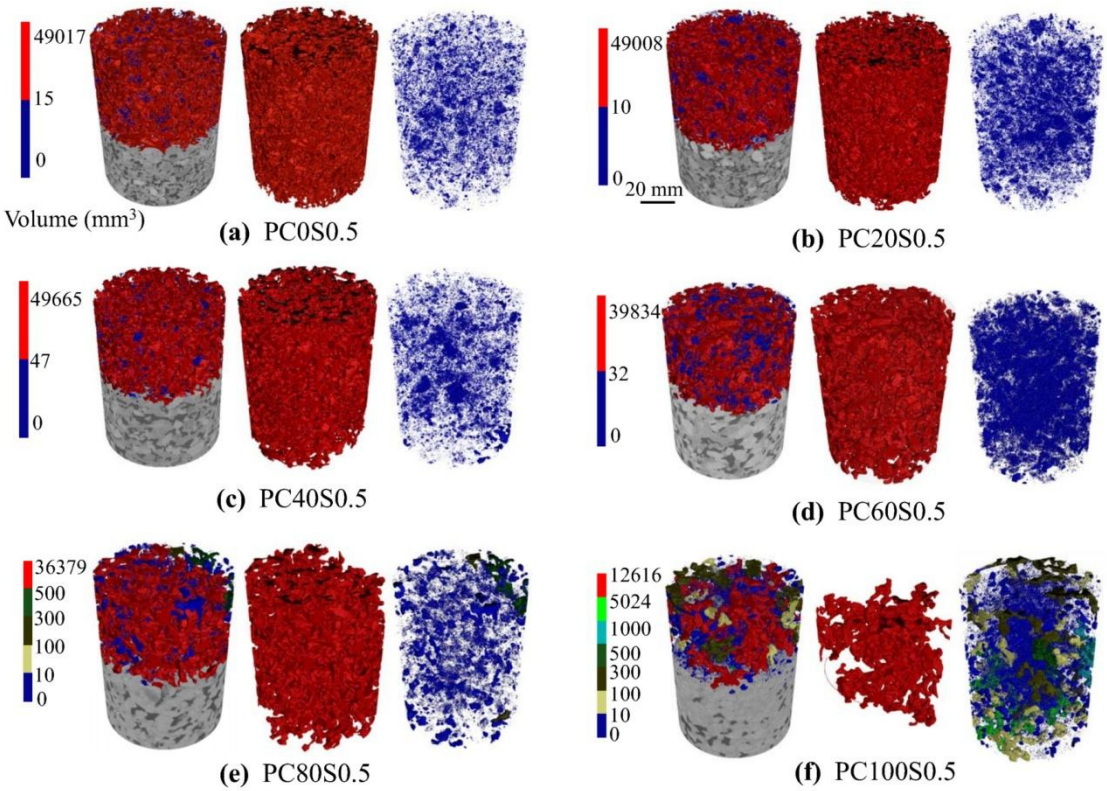

Figure 9. 3D pore structure resolved by XCT for (a) PC0S0.5, (b) PC20S0.5, (c) PC40S0.5, (d) PC6S0.5, (e) PC80S0.5, and (f) PC100S0.5 (left: overview of 3D pore structure; middle: connected pores; right: isolated pores).

The obvious changes in connected porosity and pore fraction with the BCDR aggregate substitution can be evidently explained by the results of XCT. Fig. 9c-e selectively demonstrates the sectional XCT images of the PC0S0, PC60S0.5 and PC100S0.5 samples. Clearly, the pore areas (shown as the dark phase according to the X-ray attenuation laws) decrease, suggesting the progressive elimination of the pore phase. For the PC100S0.5 sample, most of the area is occupied by the solid phases

411 including aggregates and cement mortar (Fig. 8e), which accounts for the rapidly
412 decreased connected porosity (Fig. 8b) and water permeability (Fig. 7).

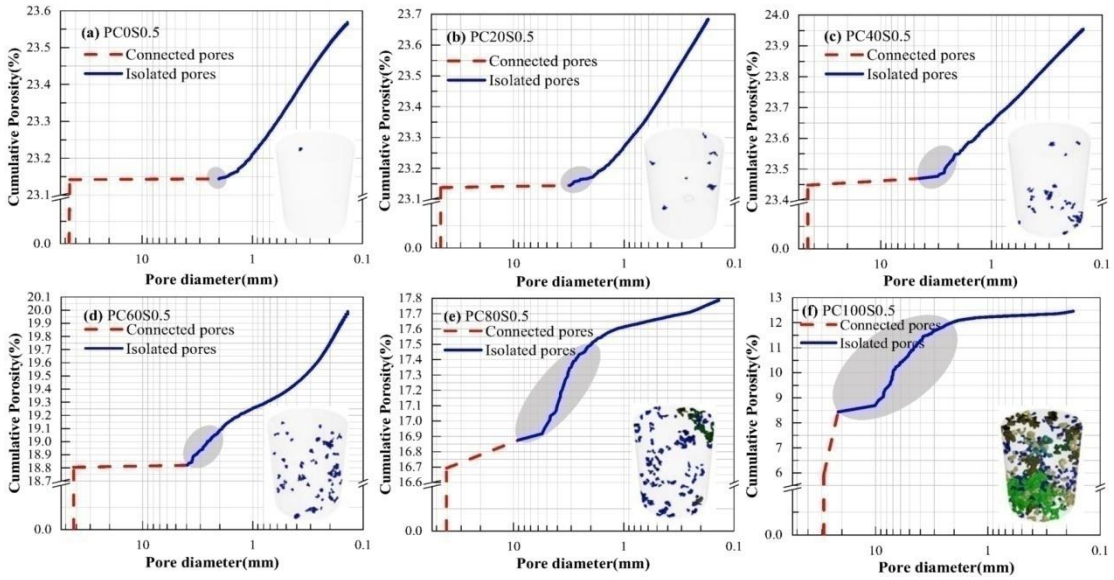

413

414 **Figure 10.** Pore size distribution and pore morphologies of the kneeling areas of pervious concrete at
415 S/C=0.5: (a) PC0S0.5, (b) PC20S0.5, (c) PC40S0.5, (d) PC6S0.5, (e) PC80S0.5, and (f) PC100S0.5.

416 3D pore structure of the pervious concrete cylinders at S/C=0.5 is shown in Fig.
417 9, where the XCT-resolved pores are classified as the connected and isolated pores,
418 and illustrated in different colors. Visually, the connected pores seem to
419 homogenously occupy the entire spaces of the pervious concrete cylinders except for
420 the PC100S0.5 sample (Fig. 9f). As the natural aggregate ratio increases, the
421 connected pore areas decrease, whereas both the distribution intensity and size of the
422 insolated pores increase (Fig. 9). The almost complete connection of the large pore
423 clusters allows the permeation of water through the concrete (Fig. 7). Rigorous
424 examination suggests that the changes of the isolated pores mainly occur at the size
425 over 2 mm, while the porosity of those below 2 mm is always less than 1% (Fig. 10).
426 In Fig. 10a-f are specifically displayed the isolated pores in the kneeled areas between

the connected and isolated pores in PoSD curves. For PC100S0.5, the big isolated porosity is increased by 4.5% (Fig. 10f). The great rises in volume fraction of the large isolated pores (> 2 mm) would naturally decrease the water permeability. These observations are in line with the findings reported elsewhere (Yu et al., 2019).

3.4 Cement mortar thickness

The thickness of cement mortar coating on aggregates was calculated based on imaging analysis on local sectional XCT images. As an example, Fig. 11a displays a selected sectional XCT image of the PC0S0.5 sample and a local magnified area including a crushed brick, cement mortar coating, and pores. Due to the gradients of X-ray attenuation density between different phases (Qi et al., 2021; Zeng et al., 2019), different gray values appear. The areas with medium, high and low gray values represent the brick aggregate, cement mortar layer, and pore in a selected area, respectively (Fig. 11b).

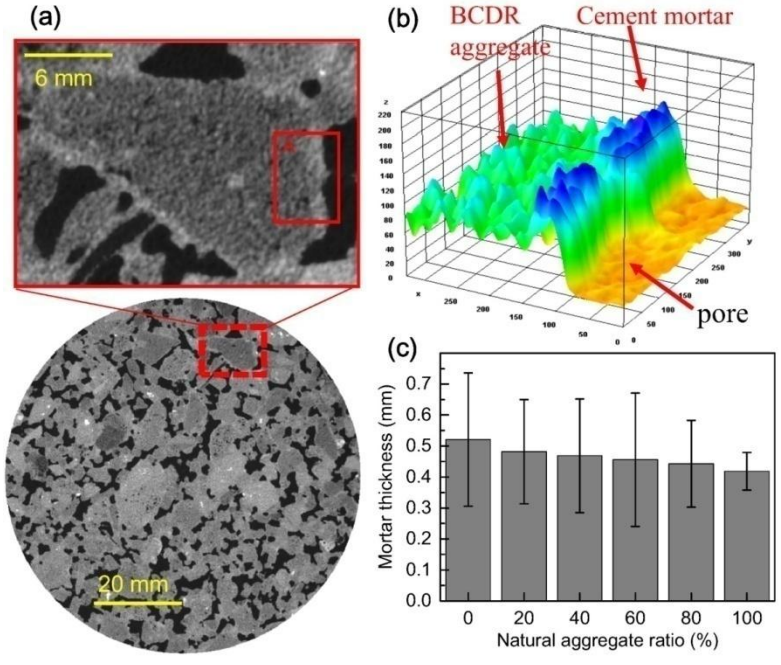

Figure 11. (a) Cross-sectional view of a PC60S0.5 sample and a representative BCDR aggregate, (b) gray value distribution of a local area in the BCDR aggregate, and (c) the statistical thickness of cement mortar on aggregate.

Thickness data of the cement mortar layer from statistic analysis for the pervious concrete mixes at S/C=0.5 are shown in Fig. 11c. As the natural aggregate ratio increases from 0% to 100%, the cement mortar coating thickness decreases slowly and linearly from 0.52 mm 0.41 mm. The relatively thin cement mortar thickness helps to prevent the clogging of connected pores (Xie et al., 2018). The higher mortar layer thickness on BCDR aggregate may be attributed to the rougher surfaces that are likely to attach more cement mortar (Tu et al., 2006, Etxeberria et al., 2007).

3.5 SEM/BSE/EDS outcomes

BSE images in different magnifications of the pervious concrete specimens are selectively displayed in Fig. 12. Within the same mechanisms of phase reorganization in XCT, in BSE images, a phase with higher density (or higher atomic number) is also displayed in a higher brightness (Peng et al., 2020; Zeng et al., 2021). So it is easy to identify the pores with the lowest brightness, the natural aggregate with the highest brightness, and the BCDR particles with the medium brightness (Fig. 12a-c). Due to the limited cement hydration extents, the new mortar contains bright spots that are the unhydrated cement clinkers. For the selected samples, the new cement mortar coats the surfaces of the BCDR and/or natural aggregates, fill the gaps and bond them together to form continual skeletons. A crack appears along the ITZ between the new cement mortar and a recycled mortar aggregate for the PC0S0.5 sample (Fig. 12d),

probably owing to the relatively large material shrinkage. No obvious porous phase is found in the ITZs for the other samples, suggesting the relatively tight matrix-aggregate interactions (Fig. 12d-f).

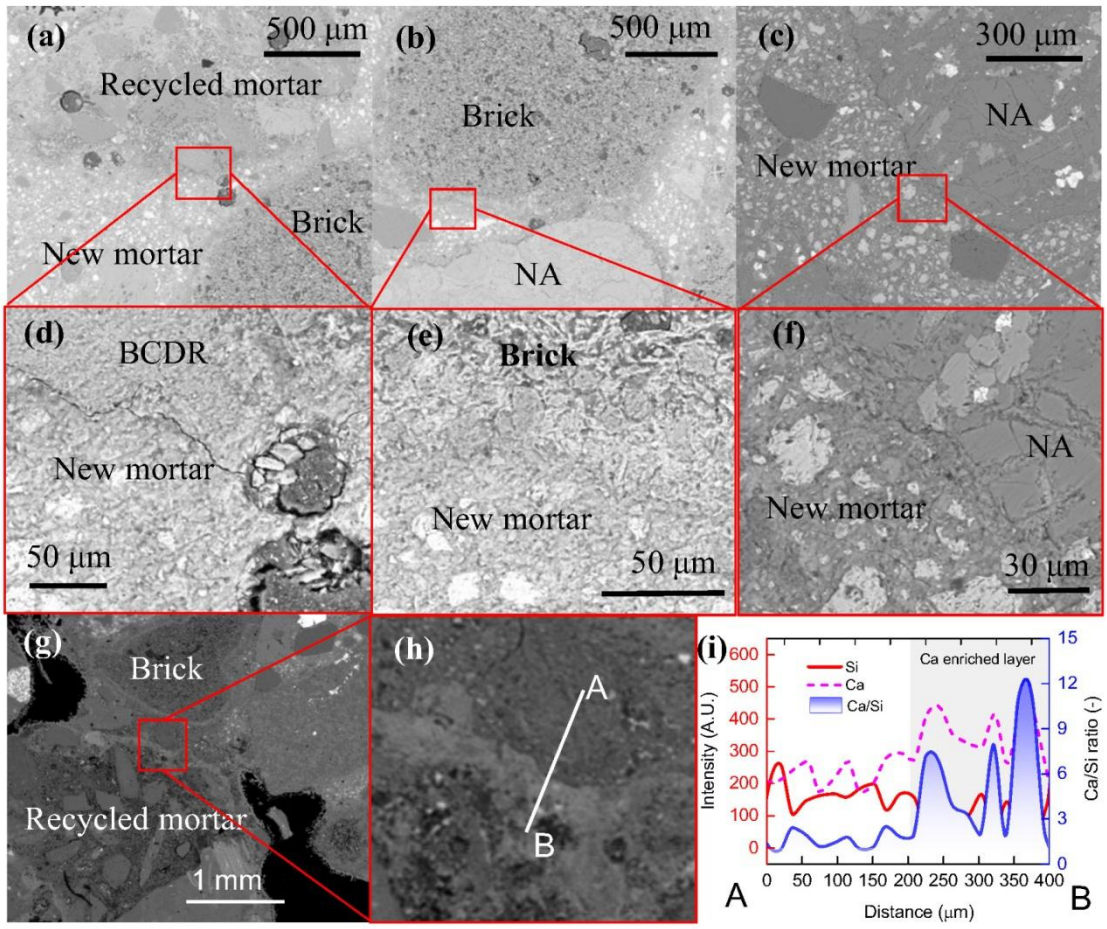

Figure 12. SEM/BSE results of PC0S0.5 (a, d), PC40S0.5 (b, e), PC100S0.5 (c, f), and local component distribution of PC0S0.5 (g, h) with the element distributions of Ca and Si, and Ca/Si ratio (i) (NA: natural aggregate).

Bright rims around BCDR aggregates were occasionally observed in BSE images. As shown in Fig. 12g, both the recycled mortar and brick aggregates show bright rims. EDS line scans crossing a bright rim indicate the high calcium content (Fig. 12h and i). In the new mortar area, the Ca/Si ratio ranges between 0.9 and 2.4 with the average

value of 1.5, in line with the generally knowledge of Ca/Si ratio for ordinary cement concrete (Kunther et al., 2017; Li et al., 2019). In the bright rim, the Ca/Si ratio is greatly and shapely raised (3~12). This Ca-enriched layer may be caused by the promoted nucleation and growth of calcium hydroxide on the rough surfaces of BCDR aggregate.

3.6 Relationship between engineering properties

Fig. 13 displays the relationships between water permeability, compressive strength, porosity and density. The water permeability generally decreases nonlinearly with the increase of compressive strength, which conforms to an exponential decaying function (Fig. 13a). Similar trends are reported in the literature (Cui et al., 2017; Oz, 2018). According to this function, the maximum compressive strength should be less than 30 MPa to conform a water permeability threshold of >0.01 cm/s, and the maximum water permeability should be less than 0.06 cm/s to conform a strength threshold of >10 MPa (Fig. 13a).

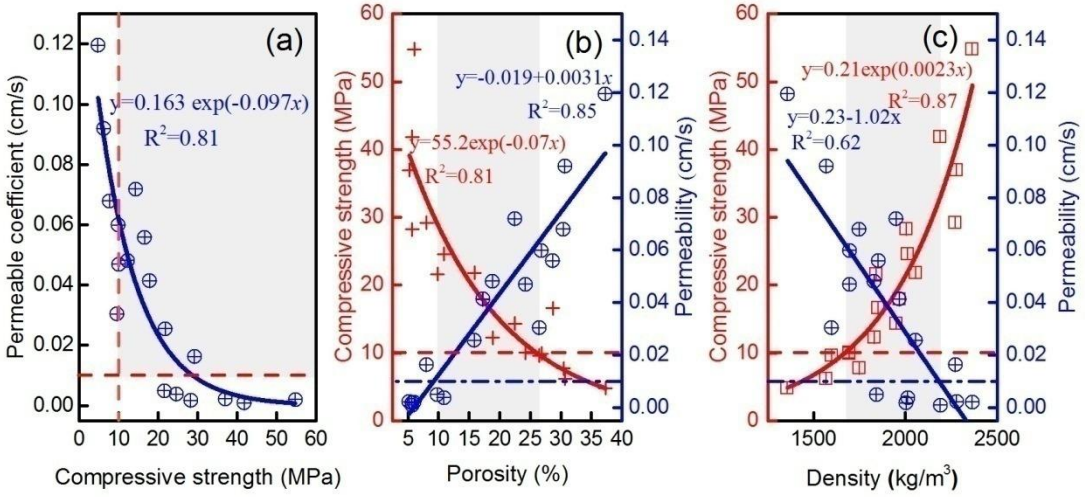

Figure 13. Plots of (a) permeability versus compressive strength, (b) compressive strength and permeability coefficient versus porosity, and (c) compressive strength and permeability versus density.

For pervious concrete design, the controls of total porosity and density are necessary. The correlations of the engineering performances (compressive strength and water permeability) with porosity and density are plotted in Fig. 13b and c. The compressive strength decreases nonlinearly with the increase of total porosity, but the water permeability-porosity plot almost follows a linearly increasing law (Fig 13b). By the contrast, a linearly decaying relationship between compressive strength and density, and an exponentially increasing relationship between water permeability and density are observed (Fig. 13c). Again, the compressive strength and water permeability thresholds (10 MPa and 0.01 cm/s) allow us to identify the confidential porosity interval of 10 ~ 26% and density interval of 1650~2150 kg/m^3. The obtained porosity interval is lower than the porosity range reported in the literature (15 ~ 35%) (Deo and Neithalath, 2010; Putman and Neptune, 2011). This suggests that a lower total porosity is required to improve concrete strength if BCDR is used for concrete fabrication.

3.7 Assessment of sustainability and economy

The sustainability of the pervious concrete mixes was assessed by equivalent CO_2 (CO_2-eq) emissions. The CO_2-eq indexes of cement, natural aggregate, recycled aggregate and sand are 0.82, 0.046, 0.0212 and 0.0139 kg/kg (Alnahhal et al., 2018; Yap et al., 2018). According to the mix proportions, the CO_2-eq emissions for

producing one cube meter of pervious concretes are shown in Fig. 14a. Clearly, as the natural coarse and/or fine aggregate content increases, the CO_2-eq emissions increase. When natural aggregate ratio rises from 0% to 100% for the pervious concrete mixes at S/C=0, the CO_2-eq emissions increase by 59.3%. Meanwhile, the CO_2-eq emissions increase by 35.3% when S/C ratio is raised from 0 to 1. Take the pervious concrete mix PC40S0.5 as an example, producing one cube meter of PC40S0.5 concrete will reduce 107 kg CO_2-eq emissions, compared with that of PC100S0.5 (Fig. 14b). The use of recycled BCDR aggregate is able to attain sufficient CO_2 emission reduction and save nature aggregate resources.

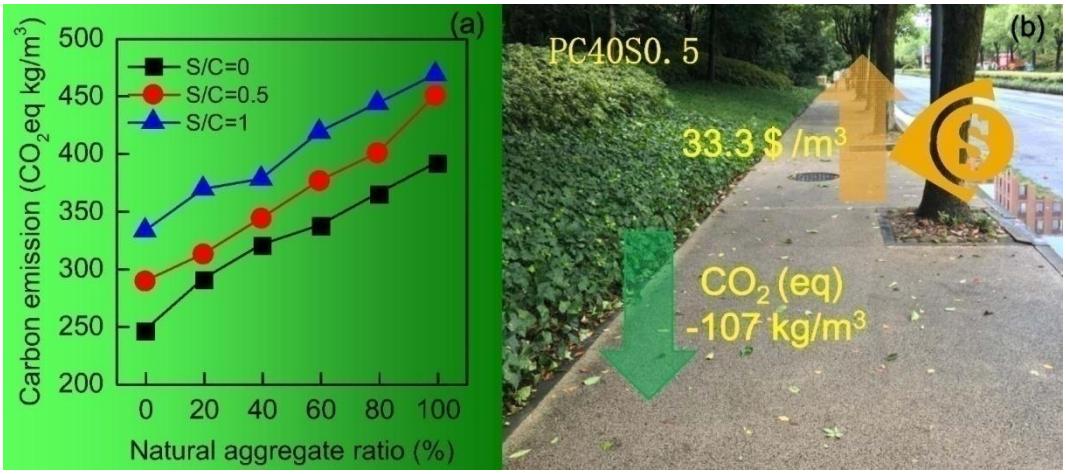

Figure 14. (a) Equivalent CO_2 emission of all pervious concrete mixtures and (b) the benefits of sustainability and economy for the optimal pervious concrete PC40S0.5.

The substitution of nature aggregate by BCDR aggregate not only improves concrete sustainability, but also brings considerable economic benefits. The local market prices of PO42.5 cement, nature coarse aggregate, fine aggregate (river sand) are 85, 18.5 and 26 USD/ton, respectively (CCPIP, 2021), so producing one cube meter of pervious concrete with pure natural aggregate (PC100S0.5) is estimated to be

73.6 USD/m^3 (equal to 476 RBM/m^3). When BCDR aggregate is used, the price will significantly decrease. BCDR is generally regarded as a type of solid waste at present, and the prices for the transport and treatment in landfill are estimated as 5.5 USD/ton. This means that using one ton BCDR aggregate can save 5.5 USD during concrete manufacture. Therefore, for the pervious concrete mix of PC40S0.5, the total cost is 40.3 USD/m^3, lower than that of PC100S0.5 by 30.3 USD/m^3 (Fig. 14b). The huge price gap will bring more profits to concrete plants if more BCDR aggregate is recycled in concrete manufacture.

Based on the data of engineering properties, environmental benefits and cost reductions, the BCDR pervious concrete mixes of PC80, PC20S0.5, PC40S0.5, PC60S0.5 and PC80S0.5 with the strength > 10 MPa and water permeability > 0.01 cm/s (level B according to GB/T25993-2010) can be adopted for engineering applications. These pervious concrete mixes are especially suitable for the infrastructures with non-heavy loads, such as, bike lanes and sidewalks, squares; parking areas, and trails. In these cases, great BCDR aggregate consumption would relax the environmental stresses caused by the continual pileup of ~~CD~~ CDW residues. However, it is worthy to mention that the relative low compressive strength may limit the application scenarios of BCDR aggregate, specific materials designs and rigorous engineering performances controls are therefore required before the in-situ concrete manufacture and engineering applications.

4. Conclusion

549 This work attempts to develop green sustainable pervious concrete with
550 secondarily recycled low-quality BCDR. With comprehensive experimental
551 investigations, the following conclusions can be drawn:

552 (1) The pervious concrete with 100% BCDR fine aggregate has low compressive
553 strength. Both the addition of sand and the substitution of BCDR aggregate by
554 natural aggregate can substantially promote the compressive strength, increase the
555 apparent density, but decrease the water permeability. The optimal concrete mixes
556 with S/C=0.5 and the BCDR aggregates ratios between 40% and 80% conform to
557 the strength and permeability requirements (>10 MPa and >0.01 cm/s).

558 (2) Increasing the natural aggregate content can decrease the total porosity and
559 connected porosity, but increase the isolated porosity. The pervious concrete with
560 100% natural aggregate has the connected porosity of 8.5% and isolated porosity
561 of 4%, compared with the concrete with 100% BCDR aggregate showing the
562 connected porosity of 23% and isolated porosity of 0.4%. The cement mortar
563 coating thickness decreases from 0.52 mm 0.41 mm, as the BCDR aggregate ratio
564 decreases from 100% to 0%. A Ca-enriched layer is found on some BCDR
565 aggregates due to the enhanced calcium hydroxide formation on rough surfaces.

566 (3) The permeability-strength, strength-porosity and strength- density relationships
567 follow exponential functions, while the permeability-porosity and permeability-
568 density relationships conform to linear functions. The confidential porosity
569 interval and density interval are 10 ~ 26% and 1650 ~ 2200 kg/m^3, respectively.

(4) The substitution of natural aggregate by BCDR aggregate can substantially decrease the equivalent CO_2 emissions and concrete production prices. Producing one cube meter of PC40S0.5 concrete will reduce 107 kg equivalent CO_2 emissions and save the cost of 30.3 USD/m^3 compared with that of PC100S0.5. The use of recycled BCDR aggregate is able to attain sufficient reductions of CO_2 emissions and concrete manufacture costs.

Acknowledgement

The research is supported by the National Natural Science Foundation of China (No. 51878602), Key projects of National Natural Science Foundation of China (52038004), and the UCL-ZJU Strategic Partner Funds.

Reference

Abera, K.A., Manahiloh, K.N., Nejad, M.M., 2017. The effectiveness of global thresholding techniques in segmenting two-phase porous media. Construction and Building Materials 142, 256–267. https://doi.org/10.1016/j.conbuildmat.2017.03.046

ACI 522R-10, 2010. Report on Pervious Concrete American Concrete Institute

ACI 213, 2003. Guide for Structural Lightweight-Aggregate Concrete 38.

Ahmed Shaikh, F.U., Nath, P., Hosan, A., John, M., Biswas, W.K., 2019. Sustainability assessment of recycled aggregates concrete mixes containing industrial by-products, Materials Today Sustainability, 5, 100013, https://doi.org/10.1016/j.mtsust.2019.100013.

591 Alnahhal, M.F., Alengaram, U.J., Jumaat, M.Z., Abutaha, F., Alqedra, M.A., Nayaka,
592 R.R., 2018. Assessment on engineering properties and CO2 emissions of
593 recycled aggregate concrete incorporating waste products as supplements to
594 Portland cement. Journal of Cleaner Production 203, 822–835.
595 https://doi.org/10.1016/j.jclepro.2018.08.292
596 ASTM C33 / C33M-18, Standard Specification for Concrete Aggregates, ASTM
597 International, West Conshohocken, PA, 2013.
598 Bittencourt, S.V., da Silva Magalhães, M., da Nóbrega Tavares, M.E., 2021.
599 Mechanical behavior and water infiltration of pervious concrete incorporating
600 recycled asphalt pavement aggregate. Case Studies in Construction Materials
601 14, e00473. https://doi.org/10.1016/j.cscm.2020.e00473
602 Bonicelli, A., Giustozzi, F., Crispino, M., 2015. Experimental study on the effects of
603 fine sand addition on differentially compacted pervious concrete. Construction
604 and Building Materials 91, 102–110.
605 https://doi.org/10.1016/j.conbuildmat.2015.05.012
606 Braga, A.M., Silvestre, J.D., de Brito, J., 2017. Compared environmental and
607 economic impact from cradle to gate of concrete with natural and recycled
608 coarse aggregates. Journal of Cleaner Production 162, 529–543.
609 https://doi.org/10.1016/j.jclepro.2017.06.057
610 CCPIP, China Cement Price Inquiry Platform, https://price.ccement.com/ (accessed at
611 8. Jul. 2021).

612 Chaitanya, M., Ramakrishna, G., 2021. Enhancing the mechanical properties of
613 pervious recycled aggregate concrete using silica fumes, Materials Today:
614 Proceedings, 46, Part 1, 634-637, https://doi.org/10.1016/j.matpr.2020.11.549
615 Chandrappa, A.K., Biligiri, K.P., 2016. Pervious concrete as a sustainable pavement
616 material – Research findings and future prospects: A state-of-the-art review.
617 Construction and Building Materials 111, 262–274.
618 https://doi.org/10.1016/j.conbuildmat.2016.02.054
619 Chindaprasirt, P., Hatanaka, S., Mishima, N., Yuasa, Y., Chareerat, T., 2009. Effects of
620 binder strength and aggregate size on the compressive strength and void ratio
621 of porous concrete. International Journal of Minerals, Metallurgy and
622 Materials 16, 714–719. https://doi.org/10.1016/S1674-4799(10)60018-0
623 Cui, X.Z., Zhang, J., Huang, D., Liu, Z.Q., Hou, F., Cui, S.Q., Zhang, L., Wang, Z.X.,
624 2017. Experimental Study on the Relationship between Permeability and
625 Strength of Pervious Concrete. Journal of Materials in Civil Engineering 29.
626 https://doi.org/10.1061/(ASCE)MT.1943-5533.0002058
627 Debnath, B., Sarkar, P.P., 2020. Characterization of pervious concrete using over burnt
628 brick as coarse aggregate. Construction and Building Materials 242, 118154.
629 https://doi.org/10.1016/j.conbuildmat.2020.118154
630 Deo, O., Neithalath, N., 2010. Compressive behavior of pervious concretes and a
631 quantification of the influence of random pore structure features. Materials
632 Science and Engineering: A, Special Topic Section: Local and Near Surface

633 Structure from Diffraction 528, 402–412.
634 https://doi.org/10.1016/j.msea.2010.09.024
635 Duan, Z., Hou, S., Xiao, J., Singh, A., 2020. Rheological properties of mortar
636 containing recycled powders from construction and demolition wastes.
637 Construction and Building Materials 237, 117622.
638 https://doi.org/10.1016/j.conbuildmat.2019.117622
639 El-Hassan, H., Kianmehr, P., Zouaoui, S., 2019. Properties of pervious concrete
640 incorporating recycled concrete aggregates and slag, Construction and Building
641 Materials, 212, 164-175, https://doi.org/10.1016/j.conbuildmat.2019.03.325.
642 Etxeberria, M., Vázquez, E., Marí, A., Barra, M., 2007. Influence of amount of
643 recycled coarse aggregates and production process on properties of recycled
644 aggregate concrete. Cement and Concrete Research 37, 735–742.
645 https://doi.org/10.1016/j.cemconres.2007.02.002
646 GB/T 25177–2010, Recycled coarse aggregate for concrete, National Standard of
647 China (2011)
648 GB/T 25993-2010, Permeable Paving Bricks and Permeable Paving Flags, National
649 Standard of China (2010)
650 GB/T 50743-2012, Ministry of housing and urban-rural development of the People's
651 Republic of China, Code for recycling of construction & demolition waste,
652 Building Plan Press, Beijing (2012)
653 Hsieh, Y.Z., Su, M.C., Chen, J.H., Badjie, B.A., Su, Y.M., 2018. Developing a PSO-
654 Based Projection Algorithm for a Porosity Detection System Using X-RayCT

655 Images of Permeable Concrete. IEEE ACCESS 6, 64406–64415.
656 https://doi.org/10.1109/ACCESS.2018.2877157
657 Ibrahim, H.A., Goh, Y., Ng, Z.A., Yap, S.P., Mo, K.H., Yuen, C.W., Abutaha, F., 2020.
658 Hydraulic and strength characteristics of pervious concrete containing a high
659 volume of construction and demolition waste as aggregates. Construction and
660 Building Materials 253, 119251.
661 https://doi.org/10.1016/j.conbuildmat.2020.119251
662 JCT 2558, 2020. Pervious Concrete, Ministry of industry and information technology
663 of China.
664
665 Kim, H.K., Lee, H.K., 2010. Acoustic absorption modeling of porous concrete
666 considering the gradation and shape of aggregates and void ratio. Journal of
667 Sound and Vibration 329, 866–879. https://doi.org/10.1016/j.jsv.2009.10.013
668 Kunther, W., Ferreiro, S., Skibsted, J., 2017. Influence of the Ca/Si ratio on the
669 compressive strength of cementitious calcium–silicate–hydrate binders.
670 Journal of Materials Chemistry A 5, 17401–17412.
671 https://doi.org/10.1039/C7TA06104H
672 Li, Jingru, Yao, Y., Zuo, J., Li, Jinggang, 2020. Key policies to the development of
673 construction and demolition waste recycling industry in China. Waste
674 Management 108, 137–143. https://doi.org/10.1016/j.wasman.2020.04.016
675 Li, Yaqiang, Li, Yue, Wang, R., 2019. Quantitative evaluation of elastic modulus of
676 concrete with nanoidentation and homogenization method. Construction and

677 Building Materials 212, 295–303.
678 https://doi.org/10.1016/j.conbuildmat.2019.04.002
679 Liu, R., Xiao, H., Pang, S.D., Geng, J., Yang, H., 2020. Application of Sterculia
680 foetida petiole wastes in lightweight pervious concrete. Journal of Cleaner
681 Production 246, 118972. https://doi.org/10.1016/j.jclepro.2019.118972
682 Liu, Q., Singh, A., Xiao, J., Li, B., WY Tam, V., 2020. Workability and mechanical
683 properties of mortar containing recycled sand from aerated concrete blocks
684 and sintered clay bricks, Resources, Conservation and Recycling, 157, 104728,
685 https: //doi.org/10.1016/j.resconrec.2020.104728.
686 Lori, A.R., Hassani, A., Sedghi, R., 2019. Investigating the mechanical and hydraulic
687 characteristics of pervious concrete containing copper slag as coarse aggregate.
688 Construction and Building Materials 197, 130–142.
689 https://doi.org/10.1016/j.conbuildmat.2018.11.230
690 Ma, M., Tam, V.W.Y., Le, K.N., Li, W., 2020. Challenges in current construction and
691 demolition waste recycling: A China study. Waste Management 118, 610–625.
692 https://doi.org/10.1016/j.wasman.2020.09.030
693 Mehrabi, P., Shariati, M., Kabirifar, K., Jarrah, M., Rasekh, H., Trung, N. T., Shariati,
694 A., Jahandari, S., 2021. Effect of pumice powder and nano-clay on the strength
695 and permeability of fiber-reinforced pervious concrete incorporating recycled
696 concrete aggregate, Construction and Building Materials, 287, 122652,
697 https://doi.org/10.1016/j.conbuildmat.2021.122652.

698 Neithalath, N., Sumanasooriya, M.S., Deo, O., 2010. Characterizing pore volume,
699 sizes, and connectivity in pervious concretes for permeability prediction.
700 Materials Characterization 61, 802–813.
701 https://doi.org/10.1016/j.matchar.2010.05.004
702 Olofinnade, O., Ogara, J., 2021. Workability, strength, and microstructure of high
703 strength sustainable concrete incorporating recycled clay brick aggregate and
704 calcined clay. Cleaner Engineering and Technology 3, 100123.
705 https://doi.org/10.1016/j.clet.2021.100123
706 Otter, R.R., Bachner, B., Nolin, S., Weatherly, J., Brown, H.J., DiVincenzo, J.P., 2016.
707 Fly ash amended pervious concrete: a laboratory study on removal potential
708 for inorganic contaminants. IJEE 8, 12.
709 https://doi.org/10.1504/IJEE.2016.078237
710 Oz, H.O., 2018. Properties of pervious concretes partially incorporating acidic pumice
711 as coarse aggregate. Construction and Building Materials 166, 601–609.
712 https://doi.org/10.1016/j.conbuildmat.2018.02.010
713 Park, D.G., Sandoval, N., Lin, W.G., Kim, H., Cho, Y.H., 2014. A case study:
714 Evaluation of water storage capacity in permeable block pavement. KSCE
715 Journal of Civil Enginering 18, 514–520. https://doi.org/10.1007/s12205-014-
716 0036-y
717 Peng, Y., Zeng, Q., Xu, S., Zhao, G., Wang, P., Liu, X., 2020. BSE-IA reveals
718 retardation mechanisms of polymer powders on cement hydration. Journal of

719 the American Ceramic Society 103, 3373–3389.
720 https://doi.org/10.1111/jace.16982
721 Putman, B.J., Neptune, A.I., 2011. Comparison of test specimen preparation
722 techniques for pervious concrete pavements. Construction and Building
723 Materials 25, 3480–3485. https://doi.org/10.1016/j.conbuildmat.2011.03.039
724 Qi, Y., Liu, K., Peng, Y., Wang, J., Zhou, C., Yan, D., Zeng, Q., 2021. Visualization of
725 mercury percolation in porous hardened cement paste by means of X-ray
726 computed tomography. Cement and Concrete Composites 122, 104111.
727 https://doi.org/10.1016/j.cemconcomp.2021.104111
728 Robalo, K., Costa, H., do Carmo, R., Júlio, E., 2021. Experimental development of
729 low cement content and recycled construction and demolition waste
730 aggregates concrete. Construction and Building Materials 273, 121680.
731 https://doi.org/10.1016/j.conbuildmat.2020.121680
732 Sata, V., Wongsa, A., Chindaprasirt, P., 2013. Properties of pervious geopolymer
733 concrete using recycled aggregates. Construction and Building Materials 42,
734 33–39. https://doi.org/10.1016/j.conbuildmat.2012.12.046
735 Shen, P., Zheng, H., Liu, S., Lu, J.-X., Poon, C.S., 2020. Development of high-
736 strength pervious concrete incorporated with high percentages of waste glass.
737 Cement and Concrete Composites 114, 103790.
738 https://doi.org/10.1016/j.cemconcomp.2020.103790
739 Shen, P., Zheng, H., Lu, J., Poon, C.S., 2021. Utilization of municipal solid waste
740 incineration bottom ash (IBA) aggregates in high-strength pervious concrete.

741 Resources, Conservation and Recycling 174, 105736.
742 https://doi.org/10.1016/j.resconrec.2021.105736
743 Sherwani, A.F.H., Faraj, R., Younis, K.H., Daraei, A., 2021. Strength, abrasion
744 resistance and permeability of artificial fly-ash aggregate pervious concrete.
745 Case Studies in Construction Materials 14, e00502.
746 https://doi.org/10.1016/j.cscm.2021.e00502
747 Sun, C., Chen, L., Xiao, J., Singh, A., Zeng, J., 2021. Compound utilization of
748 construction and industrial waste as cementitious recycled powder in mortar.
749 Resources, Conservation and Recycling 170, 105561.
750 https://doi.org/10.1016/j.resconrec.2021.105561
751 Vieira, G.L., Schiavon, J. Z., Borges, P. M., da Silva, S. R., de Oliveira Andrade, J. J.,
752 2020. Influence of recycled aggregate replacement and fly ash content in
753 performance of pervious concrete mixtures, Journal of Cleaner Production, 271,
754 122665, https://doi.org/10.1016/j.jclepro.2020.122665.
755 Visintin, P., Xie, T., Bennett, B., 2020. A large-scale life-cycle assessment of recycled
756 aggregate concrete: The influence of functional unit, emissions allocation and
757 carbon dioxide uptake. Journal of Cleaner Production 248, 119243.
758 https://doi.org/10.1016/j.jclepro.2019.119243
759 Xie, X., Zhang, T., Yang, Y., Lin, Z., Wei, J., Yu, Q., 2018. Maximum paste coating
760 thickness without voids clogging of pervious concrete and its relationship to
761 the rheological properties of cement paste. Construction and Building
762 Materials 168, 732–746. https://doi.org/10.1016/j.conbuildmat.2018.02.128

763 Yang, J., Jiang, G.L., 2003. Experimental study on properties of pervious concrete
764 pavement materials. Cement and Concrete Research 33, 381–386.
765 https://doi.org/10.1016/S0008-8846(02)00966-3
766 Yap, S.P., Chen, P.Z.C., Goh, Y., Ibrahim, H.A., Mo, K.H., Yuen, C.W., 2018.
767 Characterization of pervious concrete with blended natural aggregate and
768 recycled concrete aggregates. Journal of Cleaner Production 181, 155–165.
769 https://doi.org/10.1016/j.jclepro.2018.01.205
770 Yazdani, M., Kabirifar, K., Frimpong, B.E., Shariati, M., Mirmozaffari, M.,
771 Boskabadi, A., 2021. Improving construction and demolition waste collection
772 service in an urban area using a simheuristic approach: A case study in Sydney,
773 Australia. Journal of Cleaner Production 280, 124138.
774 https://doi.org/10.1016/j.jclepro.2020.124138
775 Yu, F., Sun, D., Wang, J., Hu, M., 2019. Influence of aggregate size on compressive
776 strength of pervious concrete. Construction and Building Materials 209, 463–
777 475. https://doi.org/10.1016/j.conbuildmat.2019.03.140
778 Yu, F., Sun, D.Q., Hu, M.J., Wang, J., 2019. Study on the pores characteristics and
779 permeability simulation of pervious concrete based on 2D/3D CT images.
780 Construction and Building Materials 200, 687–702.
781 https://doi.org/10.1016/j.conbuildmat.2018.12.135
782 Zaetang, Y., Sata, V., Wongsa, A., Chindaprasirt, P., 2016. Properties of pervious
783 concrete containing recycled concrete block aggregate and recycled concrete

784 aggregate. Construction and Building Materials 111, 15–21.
785 https://doi.org/10.1016/j.conbuildmat.2016.02.060
786 Zeng, Q., Wang, X., Yang, P., Wang, J., Zhou, C., 2019. Tracing mercury entrapment
787 in porous cement paste after mercury intrusion test by X-ray computed
788 tomography and implications for pore structure characterization. Materials
789 Characterization 151, 203–215. https://doi.org/10.1016/j.matchar.2019.02.014
790 Zeng, Q., Wang, X., Yang, R., Jike, N., Peng, Y., Wang, J., Tian, Y., Zhou, C., Ruan, S.,
791 Yan, D., 2021. Transmission micro-focus X-ray radiographic measurements
792 towards in-situ tracing capillary imbibition fronts and paths in ultra-thin
793 concrete slices. Measurement 175, 109141.
794 https://doi.org/10.1016/j.measurement.2021.109141
795 Zhang, G., Wang, S., Wang, B., Zhao, Y., Kang, M., Wang, P., 2020. Properties of
796 pervious concrete with steel slag as aggregates and different mineral
797 admixtures as binders. Construction and Building Materials 257, 119543.
798 https://doi.org/10.1016/j.conbuildmat.2020.119543
799 Zhang, J., Ma, G., Ming, R., Cui, X., Li, L., Xu, H., 2018. Numerical study on
800 seepage flow in pervious concrete based on 3D CT imaging. Construction and
801 Building Materials 161, 468–478.
802 https://doi.org/10.1016/j.conbuildmat.2017.11.149
803 Zhang, J., Zhang, A., Huang, C., Yu, H., Zhou, C., 2021. Characterising the resilient
804 behaviour of pavement subgrade with construction and demolition waste under

805 Freeze–Thaw cycles. Journal of Cleaner Production 300, 126702.
806 https://doi.org/10.1016/j.jclepro.2021.126702
807 Zhang, Z.Q., Zhang, Y.F., Yan, C.G., Liu, Y.X., 2017. Influence of crushing index on
808 properties of recycled aggregates pervious concrete. Construction and
809 Building Materials 135, 112–118.
810 https://doi.org/10.1016/j.conbuildmat.2016.12.203
811 Zhong, R., Wille, K., 2016. Compression response of normal and high strength
812 pervious concrete. Construction and Building Materials 109, 177–187.
813 https://doi.org/10.1016/j.conbuildmat.2016.01.051
814 Zhou, C.Q., 2018. Production of eco-friendly permeable brick from debris.
815 Construction and Building Materials 188, 850–859.
816 https://doi.org/10.1016/j.conbuildmat.2018.08.049
817 Zhou, H.N., Li, H., Abdelhady, A.M., Liang, X., Wang, H.B., Yang, B., 2019.
818 Experimental investigation on the effect of pore characteristics on clogging
819 risk of pervious concrete based on CT scanning. Construction and Building
820 Materials 212, 130–139. https://doi.org/10.1016/j.conbuildmat.2019.03.310